Near-Field Laser-Line Pose Sensing for Absolute Localization of Mobile Robots and Handheld Tools in Construction

Pok Yin Victor Leung[1], **Alvario Cassinelli**[1] **and Miu Ling Lam**[1]

[1]City University of Hong Kong, Hong Kong S.A.R. (China)

victor.leung@cityu.edu.hk, acassine@cityu.edu.hk, miu.lam@cityu.edu.hk

Abstract -

This paper presents a low-cost, high-precision laser-line sensor designed for construction-robotics applications such as on-site tiling, leveling, and tool localization. Unlike similar projects built around custom electronics and hardware, our approach uses a off-the-shelf microcontroller with camera module and a semi-transparent projection screen to measure the vertical position of a laser line from distances of 1–6 m with sub-millimeter accuracy. We introduce a complete sensing pipeline, including controlled illumination, and subpixel peak extraction across multiple camera modes. A fully automated data-collection framework cycles through sensor resolutions, records timing jitter and peak-detection stability, and quantifies achievable measurement precision. Results show that a consumer-grade imaging system can provide consistent, high-frequency height measurements suitable for indoor construction tasks, offering an accessible alternative to specialized CCD-based receivers or high-end laser trackers.

Keywords -

Construction Robotics; Absolute Localization; Laser Plane Sensing; Digital Fabrication

1 Introduction

Precision alignment is essential in robotic construction tasks such as floor tiling, concrete smoothing, and wall rendering, where sub-millimeter tolerances are sometimes required. While many pose estimation methods exist, few can reliably achieve this level of precision, and those that can—such as laser trackers or robotic total stations—come at high cost and with significant deployment complexity. In practice, many robotic processes do not require high precision in full 6-DOF. Instead, they can be aligned relative to a fixed planar reference. Examples include controlling floor tile placement for horizontal level or guiding wall plastering tools to stay plumb.

This paper introduces a low-cost laser-plane height sensor that leverages the geometric consistency of construction-grade laser levels. The method uses a camera in combination with a near-field projection screen to detect where a laser plane intersects the screen surface. By analyzing the position of this projected line at subpixel resolution, the sensor estimates height deviation relative to the plane with high precision. This paper focuses on the design and characterization of the sensing system itself, while integration into a complete robotic workflow is left for future work.

The main contributions of this work are: (1) a reproducible open-hardware sensor comprising only a camera module, a 3D-printed housing, and a paper screen; (2) a lightweight processing pipeline including lens focusing, calibration, and real-time peak detection; and (3) an experimental evaluation of the sensor's performance across multiple resolutions and distances, demonstrating accuracy suitable for integration into on-site robotic workflows.

2 Related Work

Robotic construction applications often rely on external positioning systems to achieve high accuracy over large workspaces. Commercial systems such as robotic total stations and laser trackers offer sub-millimeter precision by optically tracking a retro-reflective target [1]. These systems have been used in mobile construction robotics to localize manipulators relative to a site-fixed reference. Similarly, ETH Zurich's Robotic Fabrication Laboratory has deployed a Nikon iGPS system to localize robots and objects in a shared workspace [2]. While these systems enable full 6-DOF pose tracking, they impose significant infrastructure demands: tripod-mounted cameras or lasers, calibrated room-scale volumes, and line-of-sight requirements. Motion capture systems provide similar accuracy in indoor settings but require multi-camera arrays mounted on trusses or frames and are less suitable for deployment in dynamic construction sites.

Marker-based vision systems have been developed as low-cost alternatives to motion capture or total station tracking. For example, a camera mounted on the robot's end-effector can detect fiducial markers placed in the construction environment [3]. However, vision-based localization methods require sufficient lighting, careful calibration of the optical system, and stable environmental geometry. Their accuracy is inherently dependent on resolution, lens distortion, and viewing angle—factors that limit their effectiveness for long-range height sensing.

Planar Laser Sensing in Field Robotics More recently, several construction robots company have developed robots with laser line sensors, rely on laser planes as spatial references. Unfortunately, many of them are not published and their methods remain undisclosed. Published examples include a mobile robot that follows a laser line projected onto a raised-floor grid, achieving 2–3 mm positioning error using a custom-built sensor tuned to the laser profile [4]. While effective for gross alignment tasks, these sensors do not support sub-millimeter resolution or customizable processing. Only until recently, a custom laser receiver was developed for detecting the intersection of a construction-grade laser plane [5]. Using custom electronics and hardware, their spinning CCD sensor array is capable of sensing a laser plane height with accuracy of 25 µm(max) and 5.5 µm(average).

Other researchers have explored triangulation-based laser systems, where static beacons emit laser patterns and mobile receivers triangulate their position. However, such systems require multiple calibrated emitters and suffer from cumulative line-of-sight and angular ambiguity issues, particularly on cluttered sites. Camera-based sensing systems have also been used to monitor structured-light patterns or detect projected lines in manufacturing. These systems often require structured lighting conditions and are not intended for on-site construction tasks or over large distances.

3 Sensor Design and Implementation

3.1 Sensor Concept

The sensor we developed detects the vertical position of a laser plane by capturing the intersection of the laser beam with a near-field projection screen. The screen is positioned orthogonally to the incoming laser plane such that the projected line appears as a nearly straight segment across the visible field. As the sensor moves relative to the laser, the projected line shifts vertically along the screen surface. Since the sensor only measures the height of the laser line within its fixed field of view, the system effectively slides the laser intersection vertically over the screen. This converts the 3D spatial deviation relative to the plane into a 1D pixel displacement observable by the camera.

3.2 Hardware Architecture

The hardware consists of three components:

- OpenMV H7 Plus microcontroller with integrated OV5640 camera sensor, which supports resolutions up to 2592×1944. The board is officially priced at USD 95, though alternative sources offer it for approximately USD 40.The stock lens is replaced with a generic 5MP HD650 M12 lens (3.5 mm focal length, f/2.8) offering a 90° horizontal and 60° vertical field of view. The lens structure follows a 2G2P configuration and is marketed as "zero-distortion." The lens is readily available online and costs approximately USD 4.
- Mechanical enclosure and screen: The microcontroller is mounted to a custom 3D-printed PLA enclosure using two screws. The enclosure maintains a fixed 20 mm spacing between the lens and the screen. The case can be fabricated using an entry-level FDM 3D printer with a 0.2 mm layer height. No supports or post-processing are required.
- The screen is cut from standard 80 g/m² printing paper and adhered to the front of the housing using adhesive tape. The visible size of the screen is 30 × 40 mm

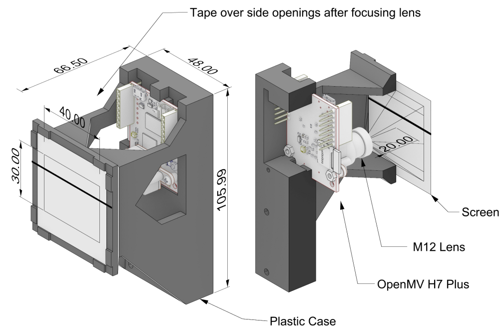

Figure 1. Dimensioned drawing (left) and cut-away (right) of the sensor hardware

After lens focusing is completed, the side openings are covered with black tape to prevent light from reaching the screen from the back side. The sensor geometry and dimensions are illustrated in Figure 1.

4 Software Architecture

The onboard firmware runs MicroPython scripts using the OpenMV IDE environment. An SD card is not required; all scripts execute from internal flash.

Lens Focusing Procedure To assist with focusing at the 20 mm working distance, a custom script is provided. The user replaces the white screen with a temporary pattern-printed paper (provided in the repository). The focus script evaluates local contrast in five image regions and computes a focus score that is displayed in real time. The user adjusts the lens manually until the score is maximized, then locks the lens in place. After focusing, the pattern is replaced with a blank screen, and all side openings are taped over to block ambient light. The focusing aid is designed to be reproducible and requires no test targets beyond the printed pattern

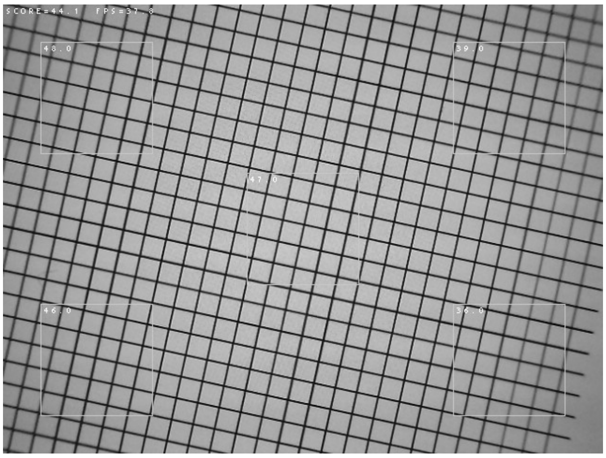

Figure 2. Frame displayed during lens-focusing. White square indicates multiple regions of interest.

Laser Line Detection Pipeline The laser detection script includes the following steps:

- Image acquisition: The sensor operates in grayscale mode at VGA resolution. Exposure and gain settings can be manually configured, though automatic exposure and gain are preferred.
- Brightness thresholding: Pixels with a brightness value below 80
- Row reduction: The captured image is collapsed into a 1-dimension vertical brightness profile. For each image row, a local mean brightness is computed using OpenMV's ROI statistics.
- Adaptive smoothing: A moving average filter is applied to the row profile. The window size is selected automatically using a statistical thresholding function (`auto_window`) that estimates the width of the bright region based on mean and variance. This step is essential for converting any flat-top area (caused by the thickness of the laser beam) into a brightness profile with well-defined peak.
- Peak detection: The smoothed profile is passed through a peak detector (`argmax`) to identify the brightest row, which corresponds to the laser line.
- Subpixel fitting: Two estimators are implemented:
  - Three-point fit: A quadratic curve is fit to the peak row and its neighbors using the standard parabola formula.
  - Five-point fit: A more robust version using five neighboring values and an approximation of a Savitzky–Golay filter, offering better stability on symmetric profiles.

The moving average smoothing helps the peak detection algorithm being insensitive to variation in image brightness. We demonstrate the robustness of the method by setting the brightness threshold to different values (from 20% to 80% at 10% increment) and confirmed that the detected peaks are identical (Fig.3). It is worth noting that the precision and repeatability produced by peak estimation does not require the laser line to have a symmetrical brightness.

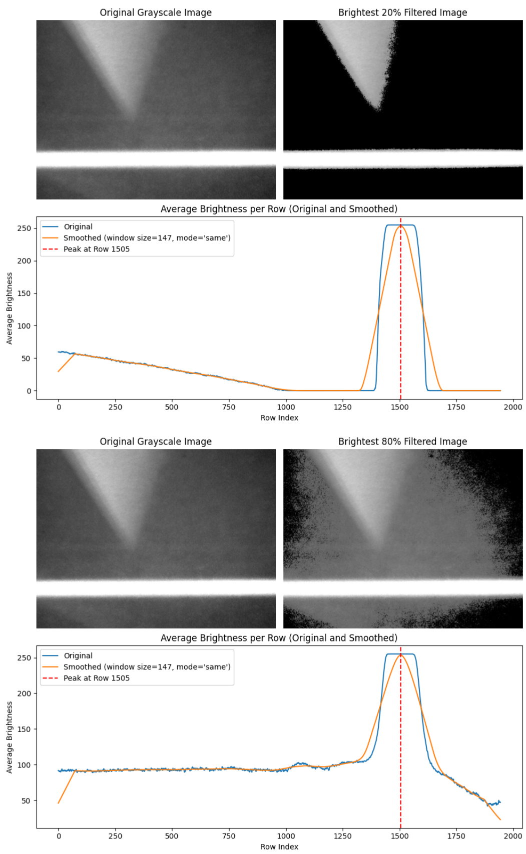

Figure 3. The project laser line (white horizontal stripe) as seen by the camera (top left) and after threshold (top right) at 20% and 80%. The brightness peak (dotted red) is identical after smoothing (orange) the raw brightness data (blue).

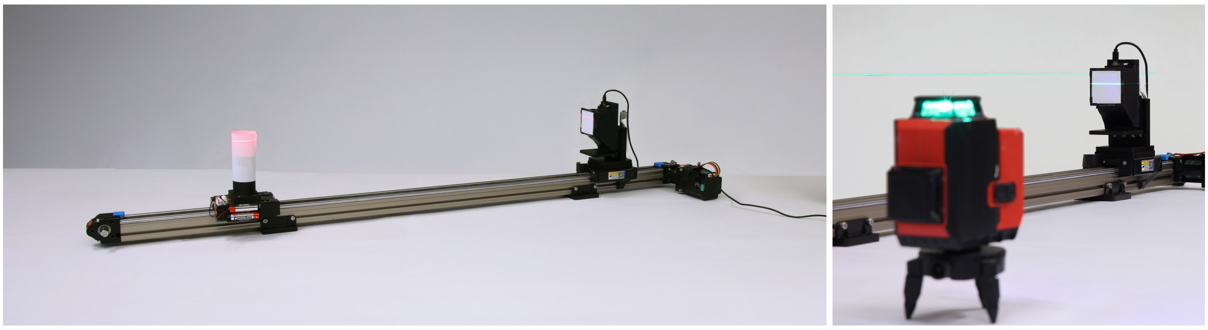

Figure 4. Photo illustrating Experiment Setup S1 (left), S2 and S3 (right)

Table 1. Overview of datasets used in evaluation, including varied parameters, spatial ranges, and emitter configurations. Emitter types are defined as S1–S3 in Section 5.1.

ID	Purpose	Resolution	z Range (mm)	d Range (mm)	Setup	Notes
T3	Precision, estimator comparison	7 res.	0–1.0	400	S1	Dense sweep (§5.2–5.3)
T4	Calibration linearity	7 res.	0–14.0	400	S1	Calibration (§5.1)
T6	Short-range emitter distance	VGA	5.0 (fixed)	60–860	S1	Emitter sweep (§5.4)
T7	Long-range (Vibration)	VGA	0–10.0	8000–13000	S2	Jitter (§5.5)
T8	Long-range (Vibration)	VGA	0–16.0	5000–8000	S3	Jitter (§5.5)
T9	Long-range (Concrete Floor)	VGA	5.0 (fixed)	1000–11000	S2	Jitter (§5.5)

5 Experimental setup

To evaluate the accuracy, stability, and geometric response of the sensor across a wide range of conditions, a set of structured experiments was conducted. These tests were designed to isolate variables such as image resolution, emitter distance, ambient lighting, and laser beam geometry, and to quantify their effect on the sensor's measurement performance.

5.1 Data Collection Apparatus

Experiments were conducted using combinations of a motorized linear size (for varying emitter distance, d), manual micrometer stage (sensor height, z), fixed or pendulum-mounted laser emitters, and varying site conditions. Three types of laser emitter setups were used (also refer to Figure 4): **S1**: Static red laser emitter on linear track: used in T3, T4, and T6 for controlled Z-sweeps and emitter-distance tests. **S2**: Pendulum green laser level (construction grade): used in T7, T9, and T10 for long-range jitter and linearity tests under passive self-leveling conditions. **S3**: Stationary green laser level: used in T8 for comparison against pendulum-based emitters on raised flooring. Ten datasets (T1 to T10) were collected during development (see Table 1); Note 1: T1, T2, and T5 were later discarded due to instability or redundancy. The remaining seven datasets (T3, T4, T6–T10) are used throughout the evaluation. Note 2: "7 res." indicates resolution sweep across QQVGA (160x120) to WQXGA2 (2592x1944).

6 Results and Discussion

6.1 Calibration linearity across resolutions

To verify the geometric behavior of the sensor, we evaluate whether the relationship between sensor height z and detected laser line position is linear across all resolutions. Dataset T4 was collected by sweeping z from 0 to 14 mm (in 15 steps) using a micrometer stage, while cycling through seven resolutions at each height. For each resolution, the mean subpixel peak position (using 3-point subpixel estimator) was fit with a linear regression against ground-truth z, and residuals (representing error) were computed per sample (in µm). Figure 5 shows the calibration lines and residuals for all resolutions. Results confirm consistent linearity across the entire range, with residuals bounded within ±20 µm.

6.2 Subpixel estimator comparison

We compare three peak detection methods: integer row index, 3-point quadratic fit, and 5-point fit. Using dataset T3 (dense 101-step Z sweep at VGA), each method's peak position is compared against the calibration curve from T4, and RMS residuals are computed. Figure 6 plots RMS error (µm) and normalized linearity error for each method and resolution. Integer peak performs worst (50–60 µm

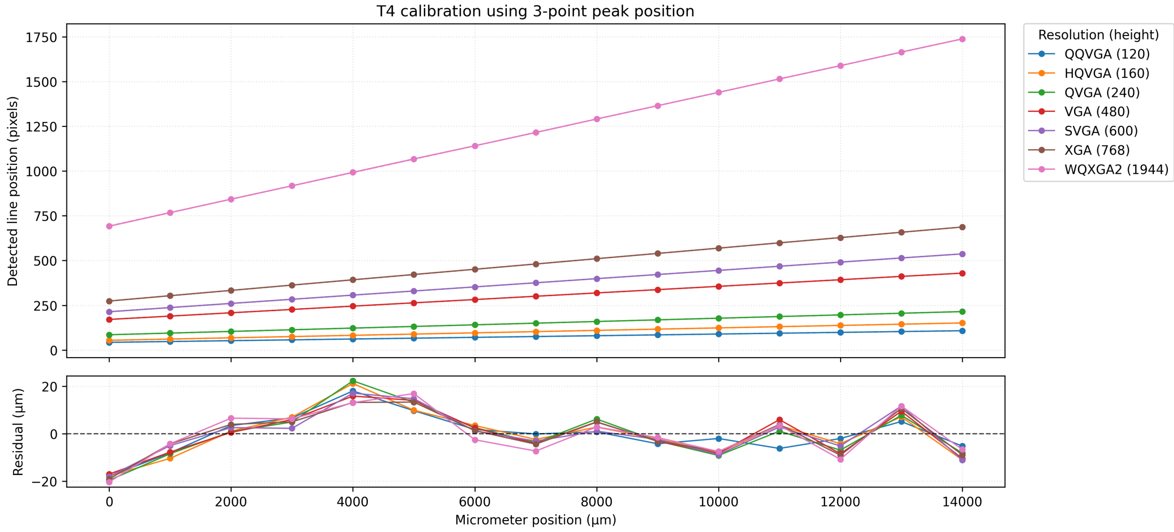

Figure 5. Calibration curves and residuals for all resolutions (dataset T4).

error), 3-point significantly improves accuracy (8–12 µm RMS), and 5-point yields no meaningful gain. The 3-point fit is therefore optimal.

6.3 Measurement error distribution at VGA

To characterize noise in a typical usage case, we analyze residual errors at VGA resolution using dataset T3. Measured heights are compared to the linear fit from T4, and residuals are converted to µm. Figure 7 shows a histogram of residuals along with symmetric percentile intervals. The median error is near zero; 90% of samples lie within ±38 µm and 95% within ±51 µm. The distribution is non-Gaussian with heavy tails but centered and repeatable. This defines the practical noise floor for VGA.

6.4 Sensitivity to emitter distance (short range)

Dataset T6 varies emitter distance from 60 mm to 860 mm while keeping sensor height fixed. At each distance, the laser line is detected and its height computed using calibration from T4. Figure 5.4 shows the mean deviation and frame-to-frame jitter versus emitter distance. A slow drift (200 µm) is observed over 800 mm, attributed to mechanical straightness of the linear track. Frame jitter remains low (¡10 µm), confirming that emitter distance has negligible impact on local precision within 1 m.

6.5 Long-range jitter on different floor types

To evaluate long-range performance under realistic conditions, we compare datasets T7–T9. The sensor is positioned at a fixed height (fixed micrometer) observing a laser emitter at large distances (up to 13m). At each testing condition, multiple observations were made (T7, T8: 10 samples; T9: 200 samples) to compute the jitter. Figure 9 shows jitter vs. distance on raised floor (T7–T8) and concrete floor (T9). The raised floor amplifies vibration and pendulum motion, leading to jitter of 50–300 µm at 8–13 m. On concrete, remains below 32 µm, an order of magnitude more stable than the test performed on raised floor. The jitter in T9 also grows linearly with distance, indicating that environmental stability, not sensor performance, dominates long-range error.

6.6 Long-range linearity

Dataset T10 tests linearity at 6 m emitter distance using 21 micrometer height steps (0–5 mm, 50 repeats each). Figure 10 shows the linear fit and residuals. The system maintains a consistent slope with RMS residuals of 14–21 µm and no curvature. Even at long distances, geometric linearity is preserved, and measurement accuracy remains stable.

7 Discussion and Conclusion

The sensor achieves sub-millimeter accuracy across a range of distances using only low-cost, readily available components. Its performance remains highly linear across all resolutions and working distances, with 95% confidence bounds of ±0.026 mm at 400 mm and ±0.050 mm at 6 m. While long-range jitter is observed, the reason is attributed to floor stability and emitter mounting instead of the sensor's internal precision. Note that, the present evaluation was conducted in indoor conditions and does not include direct sunlight or strongly mixed artificial lighting. Dust, debris, partial occlusion, and stronger ambient light can be further evaluated in future work. Such work

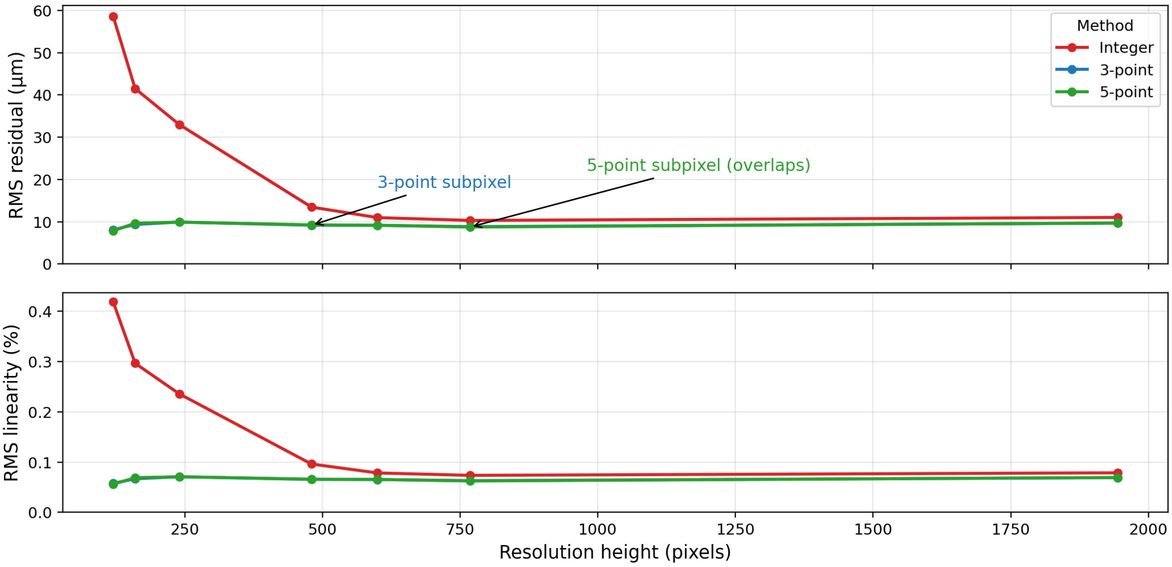

Figure 6. Comparison of integer, 3-point, and 5-point peak estimators (dataset T3). 3-point method achieves near-optimal precision with minimal complexity.

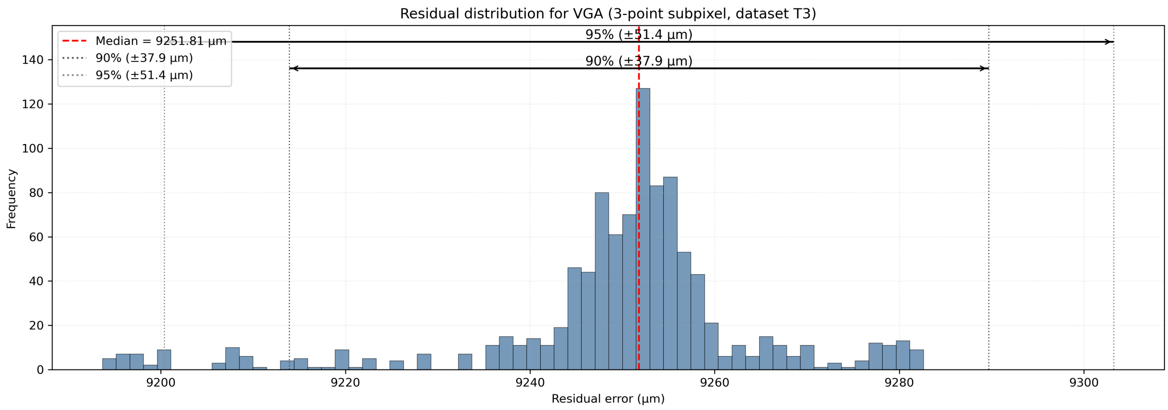

Figure 7. Histogram of residual errors at VGA (dataset T3). 90% and 95% intervals are marked with arrows; most samples lie within ±50 µm.

can try to expand towards a general hypothesis that if the human eye can discern a projected laser line in a specific environment, the camera should also be equally capable.

The measurable height span of a single sensor is bounded by the choice of screen dimensions, camera field of view, and calibration range. Thus the present prototype should be understood as one specific design while other design choices are likely possible. At longer emitter distances, usable performance is likely to be limited by laser visibility, signal-to-noise ratio and further exacerbated by environmental vibration. However, their effect is yet to be characterized.

Our method uses low-cost construction-grade laser planes as laser emitters, which lowers the financial barrier for system integration. For example, in robotic floor tiling, the sensor can be mounted on a tile gripper to regulate height relative to a site-fixed laser plane. Other sensing modules, such as accelerometers, can handle tile levelness. In addition, it also allows robots to share the same planar references used by human workers, potentially opening up new avenues for human-robot collaboration.

Our sensing method is reproducible, does not rely on optics calibration, and is intended to complement other sensors such as inclinometers or marker tracking [6]. The real-time subpixel pipeline runs entirely onboard the OpenMV camera module and requires no host computation, mak-

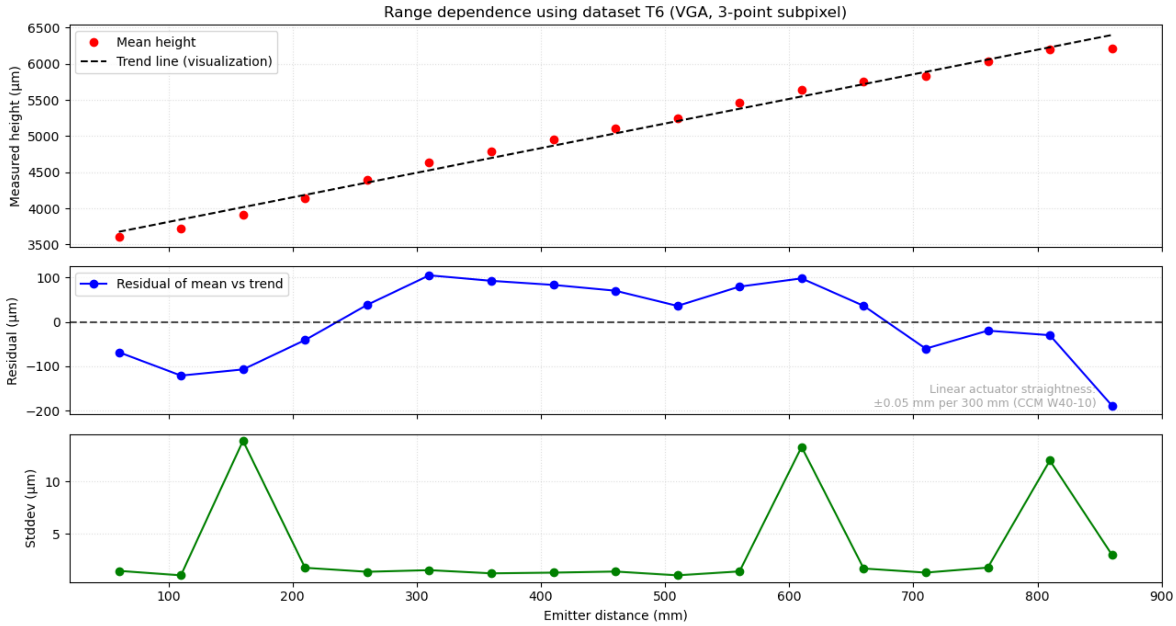

Figure 8. Measured height deviation and jitter vs. emitter distance (dataset T6). Drift remains ¡200 µm across 800 mm; jitter stays below 10 µm.

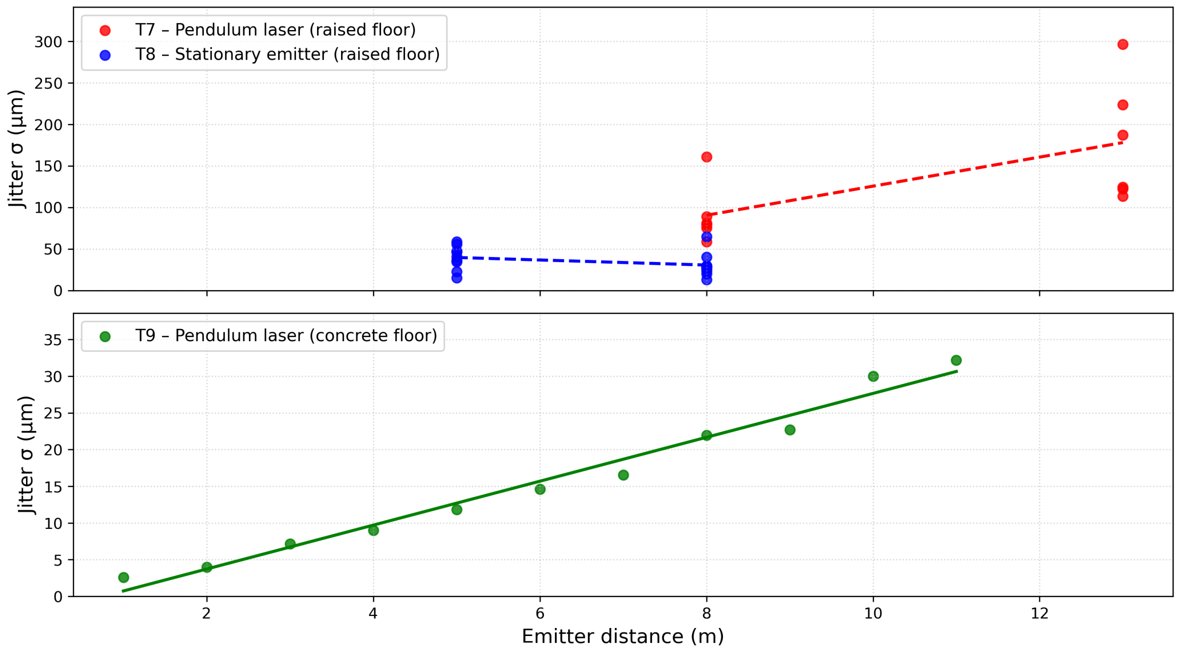

Figure 9. Long-range jitter vs. distance on different floor types (T7–T9). Tests on raised floor have large oscillations (max 300 µm); tests on concrete floor have substantially lower jitter (up to 32 µm at 11m).

ing it suitable for embedded applications. All hardware and software are released in an open-source repository `https://github.com/yck011522/laser_line_sensor/` to encourage adoption. The system avoids any custom circuit design, soldering, or firmware recompilation, and is intended to be assembled with only basic tooling and a consumer-grade 3D printer.

Future work can consider adapting the detection al-

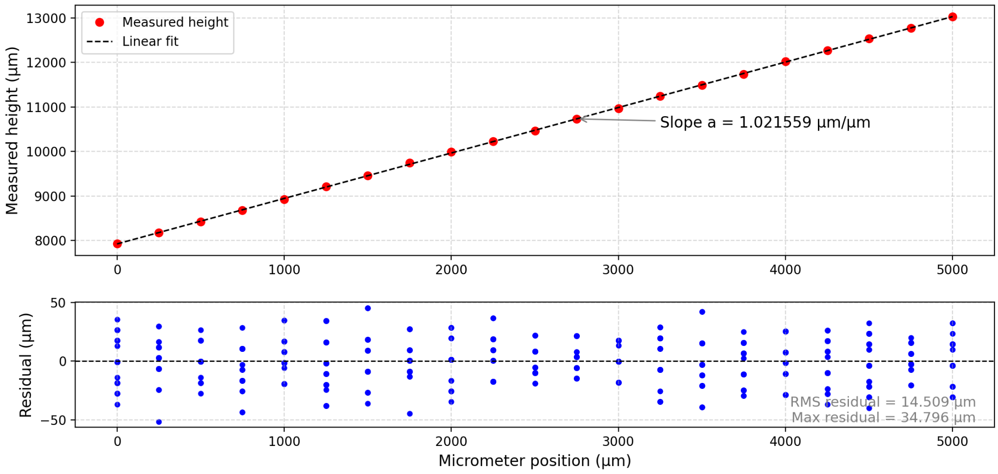

Figure 10. Linearity curve and residuals at 6 m distance (dataset T10). RMS error remains below 21 μm; no curvature or nonlinearity is observed.

gorithm to other embedded camera systems such as the ESP32-CAM or Seeed Studio XIAO ESP32S3. More broadly, the work illustrates how existing on-site tools can be reinterpreted—through near-field sensing and lightweight computation—to enable accessible precision feedback in construction robotics.

7.1 Acknowledgment

This research is supported by CityU Internal Grant 9610746.

References

[1] Selen Ercan, Sandro Meier, Fabio Gramazio, and Matthias Kohler. Automated Localization of a Mobile Construction Robot with an External Measurement Device. 2019 Proceedings of the 36th ISARC, Banff, Canada:929–936. ISSN 2413-5844. doi:10.22260/ISARC2019/0124.

[2] Manuel Lussi, Timothy Sandy, Kathrin Dörfler, Norman Hack, Fabio Gramazio, Matthias Kohler, and Jonas Buchli. Accurate and Adaptive in Situ Fabrication of an Undulated Wall Using an on-Board Visual Sensing System. In *2018 IEEE International Conference on Robotics and Automation (ICRA)*, pages 1–8. IEEE Press. doi:10.1109/ICRA.2018.8460480.

[3] Kathrin Dörfler, Timothy Sandy, Markus Giftthaler, Fabio Gramazio, Matthias Kohler, and Jonas Buchli. Mobile Robotic Brickwork. In Dagmar Reinhardt, Rob Saunders, and Jane Burry, editors, *Robotic Fabrication in Architecture, Art and Design 2016*, pages 204–217. Springer International Publishing. ISBN 978-3-319-26378-6. doi:10.1007/978-3-319-26378-6_15.

[4] Takehiro Tsuruta, Kazuyuki Miura, and Mikita Miyaguchi. Mobile robot for marking free access floors at construction sites. 107:102912. ISSN 0926-5805. doi:10.1016/j.autcon.2019.102912.

[5] Siwei Chang, Haoqian Liu, Ching-wei Chang, Nan Wang, Haobo Liang, Haitao Wu, and Guangzhen Lin. High-resolution laser receiver for construction levelling robots using multi-linear charge-coupled device (CCD) arrays. 173:106077. ISSN 0926-5805. doi:10.1016/j.autcon.2025.106077.

[6] Julian Nubert, Shehryar Khattak, and Marco Hutter. Graph-based Multi-sensor Fusion for Consistent Localization of Autonomous Construction Robots. In *2022 International Conference on Robotics and Automation (ICRA)*, pages 10048–10054. IEEE Press. doi:10.1109/ICRA46639.2022.9812386.